

Density-dependent flow in one-dimensional variably-saturated media

Michel C. Boufadel^a, Makram T. Suidan^{a,*}, Albert D. Venosa^b

^a*Department of Civil and Environmental Engineering, University of Cincinnati, Cincinnati Ohio USA*

^b*U. S. Environmental Protection Agency, National Risk Management Research Laboratory, Cincinnati, OH 45221 Ohio USA*

Received 19 July 1996; revised 14 May 1997; accepted 14 May 1997

Abstract

A one-dimensional finite element model is developed to simulate density-dependent flow of salt-water in variably saturated media. The flow and solute equations were solved in a coupled mode (iterative), in a partially coupled mode (non-iterative), and in a completely decoupled mode. Pressure head was considered as the dependent variable in the fluid motion equation, and a backward Euler scheme with mass lumping was used for time discretization of both flow and transport equations. The modified Picard method was used in the flow equation to solve for pressure heads. The model was verified by comparison to an analytical test function and published numerical results. It was found that density effects on the flow decreased with the pressure head. However, significant effects can still be observed at relatively low (negative) pressure heads. The density dependence effects were at their maxima at steady state. Partial coupling of the flow and transport equations was shown to give satisfactory results in comparison with full coupling. The advantage in partial coupling is a reduced amount of numerical computation. The finite element formulation of the model is presented in a form that allows a person with finite difference expertise to implement it easily. © 1997 Elsevier Science B.V.

Keywords: Finite Element; Beaches; Coupled-flow; Saltwater; Freshwater

1. Introduction

Flow in variably-saturated media has been investigated by many researchers (van Genuchten, 1983; Kirkland et al., 1992; Cox et al., 1994). The approach followed consists of extending Darcy's law to unsaturated media to obtain Richard's equation, and using an

* Corresponding author. Department of Civil and Environmental Engineering, University of Cincinnati, Cincinnati, Ohio, Phone # (513) 556-3695; FAX #(513) 556-2599, e-mail address: msuidan@boss.cee.uc.edu

empirical model that relates the unsaturated hydraulic conductivity and the soil moisture to pressure head (Brooks and Corey, 1966; van Genuchten, 1980a). Numerical and analytical solutions for density-dependent flows in saturated media were obtained by assuming an empirical relation between the salt concentration (usually taken as sodium chloride, NaCl) and the density of water (Henry, 1964; Segol and Pinder, 1976; Frind, 1982a, b; Galeati et al., 1992; Xue et al., 1995). To our knowledge, the only model for density-dependent flow in variably-saturated media was presented (without a detailed formulation) by Usseglio-Polatera et al. (1990). This was probably due to the lack of practical applications.

The importance of density-dependent flow in variably-saturated media has emerged following the Exxon Valdez oil spill in Alaska (Bragg et al., 1993). A better understanding of the hydraulics and the hydrodynamics in the intertidal zone of beaches in the presence of incoming fresh groundwater was needed to study dissolved nutrients transport following oil spills (Wise et al., 1994; Venosa et al., 1996). Another application arises in a different domain; Ronen et al. (1996) presented data showing upward freshwater movement from a confined freshwater aquifer to the saline unsaturated zone of the Dead Sea coastal area. Thus, there is a need for a numerical model that accounts for the effects of salt concentrations on the water density and flow.

In this paper, we develop a one-dimensional model for density-dependent flow in variably-saturated homogeneous media. The model is used to study the effects of salt concentration on water density in variably-saturated media. These effects are quantified by comparing density-dependent solutions to solutions where concentration effects on water density are neglected. A novel formulation based on the Galerkin finite element method and a backward Euler scheme is developed.

2. Problem definition

The problem of saltwater flow can be formulated in terms of the continuity equation for the fluid (mixture of fresh and sea water), a conservation equation for the salt, and a constitutive equation relating fluid density to concentration. The fluid continuity equation may be written either in terms of equivalent fresh water head (Frind, 1982a, b; Huyakorn et al., 1987) or in terms of pressure (Segol and Pinder, 1976; Voss, 1984). In this work the pressure head was used as the dependent variable because most empirical models for unsaturated flows provide the hydraulic conductivity and the soil moisture in terms of pressure heads (van Genuchten, 1980a; Rossi and Nimmo, 1994). Following the definition of Frind (1982a, b), the density difference ratio, ϵ , is expressed as

$$\epsilon = \frac{\rho_{\max} - \rho_0}{\rho_0} \quad (1)$$

where ρ_0 is the fresh water density [ML^{-3}], and ρ_{\max} is the density corresponding to the maximum salt concentration. The constitutive relation is written as

$$\rho = \rho_0(1 + \epsilon c) = \rho_0 \beta \quad (2)$$

where $\beta = 1 + \epsilon c$, and c is a dimensionless concentration (actual concentration divided by the maximum). Throughout this paper, we set $\epsilon = 0.03$ which is equivalent to a maximum seawater salt concentration of about 45 g l^{-1} (CRC, 1982). Implicit in Eq. (2) are the assumptions that conditions are isothermal and the fluid is incompressible.

The equation for the conservation of mass is

$$\frac{\partial(\rho\Phi S)}{\partial t} = -\frac{\partial(\rho q_d)}{\partial z} + \rho q \quad (3)$$

where ρ is given by Eq. (2), ϕ is the porosity of the medium, S is the saturation ratio of soil moisture with a value of 1.0 implying fully saturated soil, and q is a source/sink term [T^{-1}] that can represent uptake by plant roots and is positive if fluid is added to the system. q_d [LT^{-1}] is the Darcy flux given by Huyakorn and Pinder (1983) (p.197)

$$q_d = -\frac{k}{\mu} \left(\frac{\partial P}{\partial z} + \rho g \right) \quad (4)$$

where k is the permeability of the porous medium [L^2], μ is the fluid dynamic viscosity [$ML^{-1}T^{-1}$], P is the fluid pressure [$ML^{-1}T^{-2}$], and g is gravity acceleration [L^2T^{-1}]. Factoring $\rho_0 g$ from the quantity between parentheses, and accounting for Eq. (2), we obtain

$$q_d = -K \left(\frac{\partial \Psi}{\partial z} + \beta \right) \quad (5)$$

where $\Psi = P/(\rho_0 g)$ [L] is the pressure head and K is the hydraulic conductivity given by $K = k\rho_0 g/\mu$ [LT^{-1}]. In this derivation, it is implied that the hydraulic conductivity is independent of the salt concentration (Galeati et al., 1992; Frind, 1982a, b).

Eqs. (2)–(5) give the conservation of fluid mass which can be expressed as

$$\frac{\partial(\beta\phi S)}{\partial t} - \frac{\partial\left(\beta K \frac{\partial \Psi}{\partial z}\right)}{\partial z} = \frac{\partial(\beta^2 K)}{\partial z} + \beta q \quad (6)$$

Note that the term β^2 results from substituting ρ from Eq. (2) into Eq. (3). This substitution accounts for the spatial variation of ρ which was neglected by Galeati et al. (1992) and Frind (1982a, b). Using the van Genuchten (1980a) model, K is related to S by the following expressions

When Ψ is greater than 0.0

$$S = 1.0 \quad K = K_0 \quad (7a)$$

where K_0 is the saturated hydraulic conductivity of the homogeneous medium.

When Ψ is less than 0.0, S_e is given by

$$S_e = \frac{S - S_r}{1 - S_r} = \left[\frac{1}{1 + (\alpha|\Psi|)^n} \right]^m \quad (7b)$$

and K is given by

$$K = K_0 S_e^{(1/2)} [1 - (1 - S_e^{1/m})^m]^2 \quad (7c)$$

where $m = 1 - (1/n)$; S_r is the residual saturation ratio; α and n are model parameters determined by laboratory experiments; and $|\Psi|$ is the absolute value of Ψ .

The conservation of solute continuity equation is expressed as (Gureghian, 1983; see also p. 209 of Huyakorn and Pinder, 1983)

$$\frac{\partial(\phi S c)}{\partial t} = \frac{\partial\left(\phi S D \frac{\partial c}{\partial z}\right)}{\partial z} - \frac{\partial(q_d c)}{\partial z} + q_c \quad (8)$$

where c is the concentration of salt [ML^{-3}], q_c is a source/sink [ML^{-3}T] term that is positive for salt added to the system, and D is the dispersion coefficient as given on p. 187 of Huyakorn and Pinder (1983)

$$D = \tau D_f + a_L |V| \quad (9)$$

where D_f represents the molecular diffusion coefficient [L^2T^{-1}], τ is the tortuosity [*], V is the linear pore velocity of the fluid [LT^{-1}], given by

$$V = \frac{q_d}{\phi S} \quad (10)$$

and a_L is the dispersivity [L]. The dispersivity a_L varies with soil moisture (see p. 167 of Bear and Verrujit, 1987). But because we are not aware of any functional form, we elected to adopt the common assumption that a_L is constant (Huyakorn and Pinder, 1983).

Eqs. (6), (7a), (7b), (7c) and (8) present a highly nonlinear system. In the case where the salt is considered as a weightless tracer ($\beta = 1$) and $\Psi < 0$, nonlinearity results from Eqs. (7b) and (7c), while for $\Psi \geq 0.0$, nonlinearity resides in the variation of c which affects the values of β in Eq. (6). Hence, when these equations are solved numerically, the following approach is used: at the beginning of time step n , the concentrations are assumed known, the β terms become input to the flow equation, and an iterative scheme is used to obtain a solution for pressure heads. The Darcy flux and water velocity are computed from Eq. (5) and Eq. (10) and are factored into the transport equation Eq. (8). The transport equation is solved and the concentrations of salt are obtained; the β 's are then computed from Eq. (2). For coupled solution (IC = Iterative Coupling), the new values of β are input to the flow equation at the beginning of the same time step n , and the procedure is repeated until pressure heads and concentration obtained at the end of the time step n cease to vary (within certain precision). For partially coupled solution (NIC = Non-Iterative Coupling), the β values become input to the equation at the beginning of the following time step $n + 1$, which is a mere updating. For uncoupled solution (NC = No Coupling), β is set to 1.0 throughout.

3. Numerical implementation

In this section, we present a finite element formulation for both the water flow and the salt transport equations as given by Eq. (6) and Eq. (8).

3.1. Finite element solution of the flow equation

The flow equation was solved numerically by the Galerkin finite element method. The following variables are approximated as (Huyakorn and Pinder, 1983)

$$\Psi \cong \sum_{i=1}^N \Psi_i(t) N_i(z) \quad (11)$$

$$K \cong \sum_{i=1}^N K_i(t) N_i(z) \quad (12)$$

$$\beta \equiv \sum_{i=1}^N \beta_i(t)N_i(z) \tag{13}$$

$$S \equiv \sum_{i=1}^N S_i(t)N_i(z) \tag{14}$$

over a grid of N nodal points forming the edges of elements. Ψ_i , K_i , S_i , and β_i are pressure head, hydraulic conductivity, soil moisture ratio, and β values, at node i respectively. $N_i(z)$ is a Chapeau function that varies linearly between neighboring nodes, being 1.0 at node i and zero at all other nodes. Note that the β 's represent salt concentrations and are assumed known when solving the flow equation Eq. (6). Upon multiplying Eq. (6) by N_i , where i is a node with unknown pressure head, and integrating over the whole domain, we obtain (Huyakorn and Pinder, 1983)

$$\int_0^L \frac{\partial(\beta\phi S)}{\partial t} N_i \, dz - \int_0^L \frac{\partial(\beta K \frac{\partial \Psi}{\partial z})}{\partial z} N_i \, dz = \int_0^L \frac{\partial(\beta^2 K)}{\partial z} N_i \, dz + \int_0^L \beta q N_i \, dz \tag{15}$$

where L is the length of the domain. The transient term in Eq. (15) was computed using the mass lumping technique (Neuman, 1973). This technique, which is applied in most finite difference methods, has been shown to insure stability based on the maximum principle (Celia et al., 1990). This principle states that the maximum value of the numerical solution is dictated by either the boundary conditions or the initial data (Bouloutas, 1989). The second term on the LHS and first term on the RHS were computed using Green's formula and the second terms on the RHS was computed by direct integration. Eq. (15) can be written in the following matrix form

$$[A] \cdot \frac{d[S]}{dt} + [B] \cdot [\Psi] = [D] + [E] \tag{16}$$

where A is a diagonal matrix with terms given by

$$A_{i,i} = \rho_0 \phi \beta_i \frac{(L_{i-1} + L_i)}{2} \tag{17}$$

where L_i represents the length of element i connected to nodes i and $i + 1$. B is a tridiagonal matrix with terms given by

$$B_{i,i-1} = - \frac{\rho_0}{L_{i-1}} \left[\frac{2\beta_{i-1} + \beta_i}{6} K_{i-1} + \frac{\beta_{i-1} + 2\beta_i}{6} K_i \right] \tag{18a}$$

$$B_{i,i-1} = - \frac{\rho_0}{L_i} \left[\frac{2\beta_i + \beta_{i+1}}{6} K_i + \frac{\beta_i + 2\beta_{i+1}}{6} K_{i+1} \right] \tag{18b}$$

$$B_{i,i} = -B_{i,i-1} - B_{i,i+1} \tag{18c}$$

where the first index represent row number and the second index represents column number.

D is a vector given by

$$D_i = \rho_0 \left[- \left(\frac{\beta_i^2}{12} + \frac{\beta_{i-1}^2}{4} + \frac{\beta_{i-1}\beta_i}{6} \right) K_{i-1} + \left(- \frac{\beta_{i-1}^2}{12} + \frac{\beta_{i+1}}{12} - \frac{\beta_{i-1}\beta_i}{6} + \frac{\beta_i\beta_{i+1}}{6} \right) K_i + \left(\frac{\beta_i^2}{12} + \frac{\beta_{i+1}^2}{4} + \frac{\beta_i\beta_{i+1}}{6} \right) K_{i+1} \right] \tag{19}$$

E is a vector given by

$$E_i = \beta_i q_i \frac{L_{i-1} + L_i}{2} \tag{20}$$

where q_i is the source/sink term at node i . The formulation in Eqs. (17), (18a), (18b), (18c), (19) and (20) has not been published in the literature. It shows explicitly the effects of density dependence on water flow in variably-saturated media through the presence of the product of β and K . A major advantage of the formulation is that it presents the matrix coefficients $A_{i,i}$, $B_{i,j}$, D_i , and E_i , ($j = i - 1, i, i + 1$) in a form that is similar to the finite difference formulation where the relation between node i and the two neighboring nodes is explicitly shown. This formulation differs from the common presentation of the finite element method where the matrix coefficients are elemental (i.e. over an element) quantities (Huyakorn and Pinder, 1983). Therefore, the current formulation is easily applicable by a person with finite difference expertise, which is particularly important due to the wide spread of the finite difference method.

Using the backward Euler method for time discretization, Eq. (16) becomes a nonlinear ordinary differential equation in Ψ (S is related to Ψ via Eqs. (7a), (7b) and (7c)). This is because the terms of the B and the D terms in Eq. (16) depend on the pressure head which is yet to be determined. The A terms do not depend on pressure heads and the E terms are assumed given. Techniques for solving Eq. (16) are, among others, the Newton–Raphson method, the Implicit factoring scheme (Paniconi et al., 1988), and the Picard iteration method (Istok, 1989). In this work, Picard iteration was used due to its simplicity and stability. The method has a convergence rate of $O(d\Psi)$, which is slower than the Newton–Raphson scheme, $O(d\Psi^2)$ (see p. 153 of Huyakorn and Pinder, 1983). However, it is generally more stable (Paniconi and Putti, 1994). For each time step, the Picard iteration consists of guessing a pressure head distribution (usually the values obtained at the previous time step), computing the terms of B and D as functions of the guessed pressure distribution, and solving the resulting linear system for Ψ . The new Ψ values are used to update B and D , and a new solution is obtained. Iteration stops when the pressure head converges within a certain preset tolerance. Using k to indicate iteration level and n the time step we obtain

$$\frac{[A]}{\Delta t} [S]^{n+1,k+1} + [B]^{n+1,k} [\Psi]^{n+1,k+1} = [D]^{n+1,k} + [E]^{n+1,k+1} + \frac{[A]}{\Delta t} [S]^n \tag{21}$$

Although S is related analytically to Ψ via Eqs. (7a), (7b) and (7c), its discretized counterpart may give an erroneous mass balance. The modified Picard method developed by Celia

et al. (1990) is used because it insures general mass conservation. The key to the method lies in the expansion of $S^{n+1,k+1}$ in a truncated Taylor series with respect to Ψ , about the expansion point $\Psi^{n+1,k}$, namely

$$[S]^{n+1,k+1} = [S]^{n+1,k} + \left. \frac{dS}{d\Psi} \right|^{n+1,k} (\Psi^{n+1,k+1} - \Psi^{n+1,k}) \tag{22}$$

When Eq. (22) is inserted in Eq. (21), the resulting equation is

$$\begin{aligned} & \frac{[A]}{\Delta t} [C_p]^{n+1,k} [\Psi]^{n+1,k+1} + [B]^{n+1,k} [\Psi]^{n+1,k+1} \\ & = [D]^{n+1,k} + [E]^{n+1,k+1} + \frac{[A]}{\Delta t} [S]^n - [A][S]^{n+1,k} + [A][C_p]^{n+1,k} [\Psi]^{n+1,k} \end{aligned} \tag{23}$$

$[C_p]$ is a diagonal matrix with terms given by $C_p = dS/d\Psi$. C_p was calculated analytically using the tangent method because this method was shown to give better numerical efficiency than the standard chord slope method (Rathfelder and Abriola, 1994). Multiplying C_p by ϕ gives the well-known capacitance matrix. At each Picard iteration, the resulting system of linear equations was solved using the very efficient Thomas’s algorithm (Anderson et al., 1984).

The empirical scheme of underrelaxation developed by Cooley (1983) and adapted by Huyakorn et al. (1986) was used first. However, for the applications that we selected, instability did not occur when we set the underrelaxation coefficient equal to the upper limit of 1.0. Hence, the underrelaxation scheme was discarded.

3.2. Finite element formulation of the transport model

The salt concentration, c , was assumed to be approximated by

$$c \cong \sum_{i=1}^N C_i(t) N_i(z) \tag{24}$$

Upon multiplying Eq. (8) by N_i , where i is a node with unknown concentration, and integrating over the whole domain, we obtain

$$\begin{aligned} & \int_0^L \left(\frac{\partial(\phi \cdot S \cdot c)}{\partial t} \right) N_i \, dz - \int_0^L \left(\frac{\partial \left(\phi S D \frac{\partial c}{\partial z} \right)}{\partial z} \right) N_i \, dz \\ & + \int_0^L \left(\frac{\partial(q_d \cdot c)}{\partial z} \right) N_i \, dz = \int_0^L q_c N_i \, dz \end{aligned} \tag{25}$$

It is important at this juncture to note that S , D , and q_d are assumed known, and q_c is assumed given. The first term on the left hand side of Eq. (25) was evaluated using the mass lumping technique. Green’s formula was applied to the second term and direct integration was used for the remaining two terms. This was shown in our work to give better results for linear Chapeau functions due to the discontinuity of the Darcy flux across element interface (Galeati and Gambolati, 1989) and the ease in representing outflow boundary. Following Frind (1982a, b), q_d and D were evaluated at the middle of the

elements. Hence

$$[A_c] \frac{d[C]}{dt} + [B_c][C] = [E_c] \quad (26)$$

where $[A_c]$ is a diagonal matrix whose terms are given by

$$A_{c,i,i} = \phi S_i \frac{L_{i-1} + L_i}{2} \quad (27)$$

and $[B_c]$ is a tridiagonal matrix with terms given by

$$B_{ci,i-1} = -\frac{\phi S_i}{L_{i-1}} D_{i-1/2} - \frac{q_{di-1/2}}{2} \quad (28a)$$

$$B_{ci,i+1} = -\frac{\phi S_i}{L_i} D_{i+1/2} - \frac{q_{di+1/2}}{2} \quad (28b)$$

$$B_{ci,i} = \phi S_i \left(\frac{d_{i-1/2}}{L_{i-1}} + \frac{d_{i+1/2}}{L_i} \right) + \frac{q_{di-1/2} - q_{di+1/2}}{2} \quad (28c)$$

where $i - (1/2)$ represents the middle of element $i - 1$ located between node $i - 1$ and node i . $[E_c]$ is a vector whose term are given by

$$E_{ci} = q_{ci} \frac{L_{i-1} + L_i}{2} \quad (29)$$

Similar to the water flow formulation, Eqs. (27), (28a), (28b), (28c) and (29) are presented in a form similar to the finite difference method. The backward Euler procedure was used to integrate Eq. (26) over time and the Thomas algorithm was used to solve the linear system. Stable and oscillation free solutions of the transport model were obtained by assuring that the nodal spacing dz is such that $dz \leq 2a_L$ (Piver and Lindstrom, 1991).

4. Model verification

In this section we present four examples to test the ability of both the flow and the transport models to simulate various physical scenarios.

4.1. The flow model

4.1.1. Example 1: Simulation of consecutive draining and filling cycles

Many analytical solutions have been developed for variably-saturated flow (Broabridge and White, 1988; Warrick et al., 1991; Barry et al., 1993; Basha, 1994). However, the hydraulic conductivity–moisture–pressure head curves used for obtaining these solutions are different from Eqs. (7a), (7b) and (7c). Fitting a hypothetical $K-\theta-\Psi$ curve to an experimental curve using the method of moments was suggested by Brutsaert (1982) and used by Paniconi et al. (1988) who extended the van Genuchten curves given by Eqs. (7a),

(7b) and (7c) to eliminate discontinuity at $\Psi = 0$. We believe that the use of any estimation tool, especially the method of moments, which gives more weight to the tail of a distribution (Boufadel, 1992), will produce parameter estimation errors that should be avoided. Hence, our approach is to assume an analytical form of the solution, inputting it into Eq. (6), and computing analytically the q terms. Subsequently, these terms are used, in discretized form, as forcing terms in Eq. (23). The computed numerical solution is then compared to the assumed analytical solution.

Because of the periodic nature of tidal and wave motion on beaches, we assume

$$\Psi = -a \sin(z-t) \quad (30)$$

where z and a are given in centimeters and t in seconds. Eq. (30) represents a pressure wave of maximum amplitude a , propagating downward at the speed of 1 cm s^{-1} . Dirichlet boundary conditions were computed from Eq. (6) and applied in the numerical model (Eq. (23)). Soil properties (used throughout this paper) are adapted from Pan and Wierenga (1995) for soil 3 in their paper, namely, $n = 2.0$, $\alpha = 0.035$, $\phi = 0.368$, $S_r = 0.102/0.368$, and $K_o = 9.22 \times 10^{-3} \text{ cm s}^{-1}$. The results are plotted in Fig. 1 for $a = 2.0 \text{ cm}$. We can see from

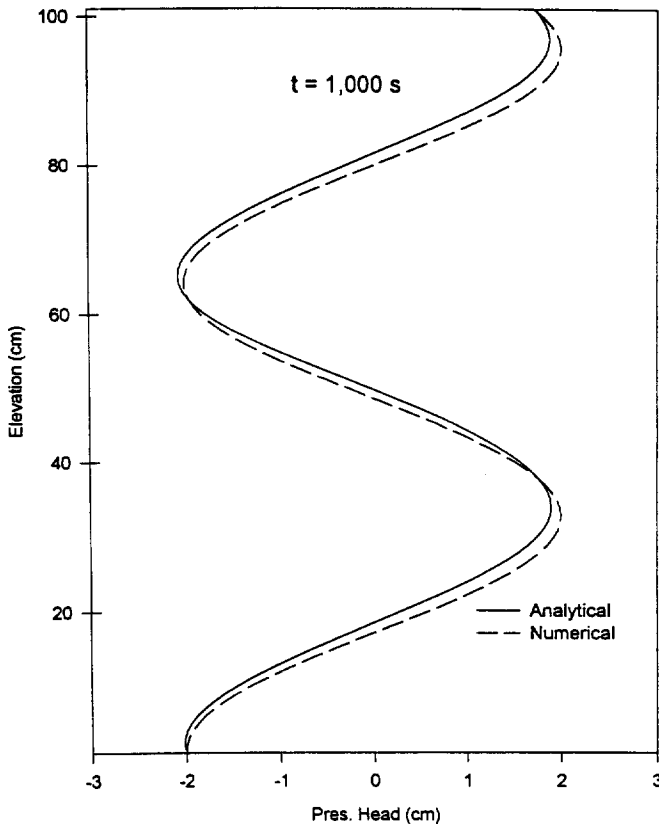


Fig. 1. Pressure head comparison between analytical test function and numerical solution.

Fig. 1 very good agreement between the analytical and the numerical solutions, considering the truncation error resulting from the large value of the space increment $dz = 1.0$ cm and the discontinuity inherent in the van Genuchten model (Eqs. (7a), (7b) and (7c)) at $\Psi = 0.0$.

4.1.2. Example 2: Simulation of very dry initial conditions

Further verification of the flow model was conducted to investigate its ability to simulate a sharp front of pressure head. This was done by comparing to Case 3.1 from Pan and Wierenga (1995). The initial condition is $\Psi(t = 0, z) = -50\,000$ cm and the boundary conditions are given by $\Psi(t, z=0) = \Psi(t, z = 100\text{ cm}) = 100$ cm. Using a time step of $\Delta t = 3.6$ s and a spatial increment $\Delta z = 1.0$ cm, the results of this simulation for $t = 180$ s are shown in Fig. 2 where good agreement occurs between the present model and Pan and Wierenga’s results. Fig. 2 shows the ability of the model to simulate large gradients of moisture and pressure head without introducing considerable numerical dissipation (smearing).

4.2. The transport model

4.2.1. Example 3: Comparison to an analytical solution for uniform soil moisture

There are no known analytical solutions to the transport equation (Eq. (8)) in the general case. However, analytical solutions are obtained for particular situations such as when the soil moisture is constant (Ogata and Banks, 1961; van Genuchten, 1981), or for conditions where physical dispersion is negligible ($D = 0.0$), (Lomen et al., 1984). We chose to test the numerical transport model against the analytical solution for the condition of a constant moisture content. This is because for $L = 100$ cm, a realistic value of a_L would be about 1 cm (Wierenga and van Genuchten, 1989); thus, dispersion cannot be neglected with respect to convection. Also, the analytical solution given by Lomen et al. (1984)

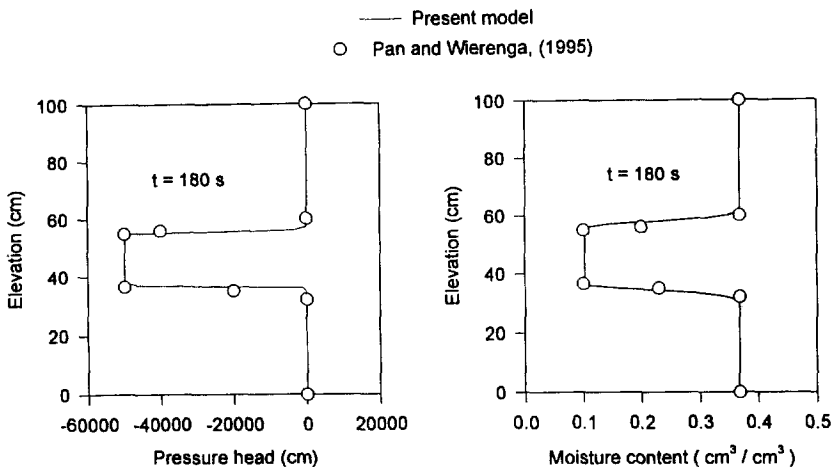


Fig. 2. Pressure head and soil moisture ratio from the very dry initial conditions case.

requires a steady state analytical solution for the flow model, which cannot be obtained for the soil properties given by Eqs. (7a), (7b) and (7c). We consider the case of $S(t,z) = 1.0$ and $q_d = 0.00922 \text{ cm s}^{-1}$ with initial and boundary values for concentration given by $c(t=0, z) = 0.0$; $c(t, z=0) = 0.0$; and $c(t, z=L=100 \text{ cm}) = 1.0$. The analytical solution for Eq. (8) subject to these conditions is given by Ogata and Banks (1961)

$$\frac{c}{c_{\max}} = \frac{1}{2} \left[\operatorname{erfc} \left(\frac{L-z+q_d t}{2\sqrt{D t}} \right) + \operatorname{Exp} \left(\frac{(L-z)q_d}{D} \right) \operatorname{erfc} \left(\frac{L-z-q_d t}{2\sqrt{D t}} \right) \right] \quad (31)$$

where erfc is the complementary error function (Abramowitz and Stegun, 1970). The diffusion term (τD_i) is set equal to $10^{-6} \text{ cm}^2 \text{ s}^{-1}$ throughout this paper except when otherwise stated. Comparison for $a_L = 1.0 \text{ cm}$ and $a_L = 10 \text{ cm}$ is shown in Fig. 3 where excellent agreement is observed.

4.3. Combined testing of both flow and transport model

4.3.1. Example 4: Water and solute transport in an unsaturated homogeneous soil

The performance of both flow and transport models in predicting water and solute transport in the absence of density dependence is further evaluated by comparing against the numerical results of van Genuchten (1980b). The numerical experiment simulates the transport of a conservative ionic species (Cl^-) in an unsaturated homogeneous soil column of length 125 cm. The uniform soil porosity was $\phi = 0.38$ and the hydraulic properties of the soil are given by the following equations with $\theta = S\phi$ (S being the soil moisture ratio)

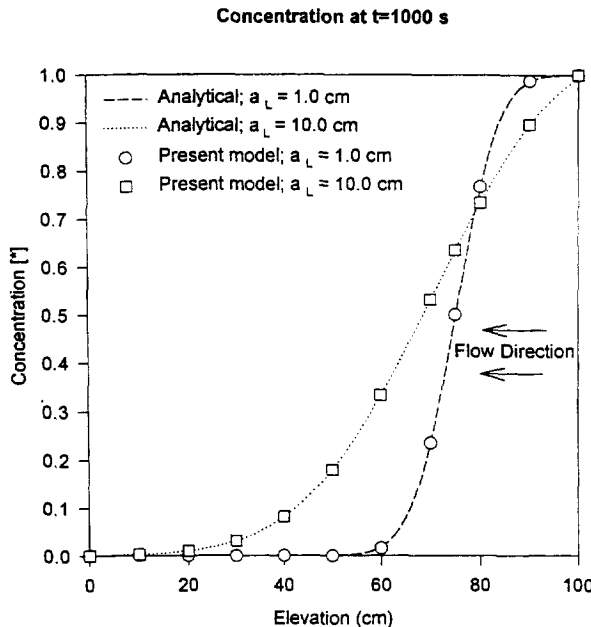


Fig. 3. Spatial distribution of concentration for two dispersivity values.

where θ expressed in $\text{cm}^3 \text{cm}^{-3}$: for $\Psi \leq -29.484 \text{ cm}$

$$\theta(\Psi) = 0.6829 - 0.09524 \text{Ln}(|\Psi|) \tag{32a}$$

$$K(\Psi) = 1.934 \cdot 10^6 |\Psi|^{-3.4095} \tag{32b}$$

for $-29.484 \text{ cm} < \Psi \leq -14.495 \text{ cm}$

$$\theta(\Psi) = 0.4531 - 0.02632 \text{Ln}(|\Psi|) \tag{33a}$$

$$K(\Psi) = 5.168 \times 10^2 |\Psi|^{-0.97814} \tag{33b}$$

where K is given in cm/day and Ψ in cm . The initial distribution for soil moisture is $\theta(t=0, z) = 0.20$ for $z \leq 65 \text{ cm}$, and $\theta(t=0, z) = 0.2542 - 8.333 \times 10^{-4}z$, for $65 < z \leq 125 \text{ cm}$. The initial pressure distribution was back-calculated from Eq. (32a). The initial chloride concentration is zero and the chloride is introduced in the domain at time $t=0$ as a 2.8 hour pulse with the following boundary conditions at the top of domain: for $t > 0.0$, $\Psi(t, z = 125 \text{ cm}) = -14.95 \text{ cm}$; for $0.0 < t \leq 2.8 \text{ hour}$, $c(t, z = 125 \text{ cm}) = 209 \text{ meq l}^{-1}$, and for $t > 2.8 \text{ hour}$ $c(t, z = 125 \text{ cm}) = 0.0$. At the bottom of the domain, outflowing boundary conditions are simulated by setting $\delta\Psi/\delta z = \delta c/\delta z = 0$ throughout the simulation. The diffusion term τD_f and the dispersivity a_L were set to $6.94 \times 10^{-6} \text{ cm}^2 \text{ s}^{-1}$ and 1.026 cm . The time step Δt and the spatial increment Δz were set at 0.096 hour and 1.0 cm , respectively.

The soil moisture distributions at $t = 2 \text{ hours}$ and $t = 9 \text{ hours}$ are shown in Fig. 4a where excellent agreement occurs between the present model and the van Genuchten (1980b) results. Fig. 4b shows the variation of the chloride concentration with space at two distinct times, as predicted by our model and van Genuchten (1980b). The good agreement

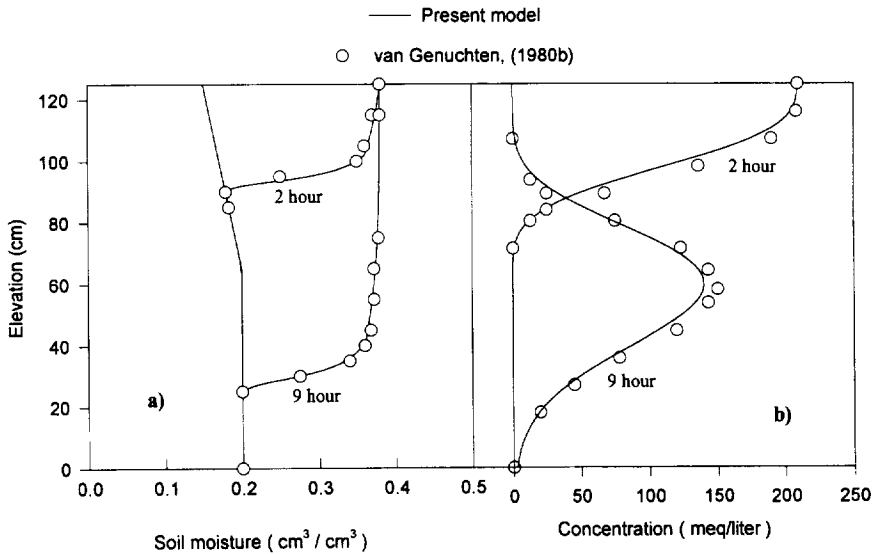


Fig. 4. a) Soil moisture and b) chloride concentration distributions at two different times.

between the two models is clearly apparent at $t = 2$ hours and $t = 9$ hours. The slight discrepancy between our model and the van Genuchten results at $t = 9$ hours is probably due to numerical dissipation (smearing). This is because, as stated in van Genuchten (1980b), his solution was obtained by increasingly decreasing the temporal and spatial increments until the simulated results cease to vary. This reduces tremendously numerical smearing which can be shown to depend on Δz^2 (see p. 90 of Anderson et al. (1984)). The effect of numerical smearing is further supported by the fact that our model overpredicts the concentration at the tail of the distribution and underpredicts it at the peak, such as to conserve mass balance.

5. Density-dependent flow

In this section, four applications of the numerical model that illustrate the error resulting from neglecting density dependence in variably-saturated media are presented. The soil parameters adapted from Pan and Wierenga (1995) for soil 3, are used throughout and the dispersivity a_L is set equal to 1.0 cm as estimated from the laboratory experiments of Wierenga and van Genuchten (1989). This section has two goals. The first goal is numerical and consists of evaluating whether IC (full coupling) is necessary to model seawater transport or NIC (partial coupling) is sufficient. Obviously, the advantage of the latter is a reduced computational cost. The second goal is physical and consists of quantifying the error resulting from neglecting the effects of concentration on water density in variably-saturated media. The sensitivity of the model to the choice of the dispersivity will be considered. The reader is reminded that the concentration values are presented in a normalized form hence $\epsilon = 0.03$ corresponds to a maximum salt concentration of around 45 g l^{-1} .

5.1. Application 1

This application is used to illustrate the effect of density dependence on Darcy's and mass fluxes at steady state.

5.1.1. Application 1-a

Pressure head initial and BC.

$$\Psi(t=0, z) = 10 \text{ cm}; \Psi_{\text{bottom}} = \Psi(t, z=0) = 10 \text{ cm}, \Psi_{\top}(t, z=100 \text{ cm}) = 10 \text{ cm}$$

Concentration initial and BC.

$$c(t=0, z) = 1.0; c(t, 0) = 1.0, c(t, 100 \text{ cm}) = 1.0$$

5.1.2. Application 1-b

Pressure head initial and BC's.

$$\Psi(t=0, z) = -1000 \text{ cm}; \Psi_{\text{bottom}} = \Psi(t, z=0) = -1000 \text{ cm},$$

$$\Psi_{\top} = \Psi(t, z=100 \text{ cm}) = -1000 \text{ cm}$$

with concentration initial and BC as given by Application 1-a.

Table 1
Darcy and mass fluxes for Case 1-a and Case 1-b

	Darcy flux/cm s ⁻¹		Mass flux/g s ⁻¹	
	NC*	NIC ⁺	NC*	NIC ⁺
Case 1-a	9.22 10 ⁻⁰³	9.4966 10 ⁻⁰³	9.22 10 ⁻⁰³	9.782 10 ⁻⁰³
Case 1-b	3.1571 10 ⁻¹⁰	3.252 10 ⁻¹⁰	3.1571 10 ⁻¹⁰	3.3494 10 ⁻¹⁰

NC*: no coupling; NIC + : Non-iterative coupling.

As expected from pressure and concentration initial and boundary conditions, $\Psi(t,z)$, and $c(t,z)$ are constant. However, the Darcy fluxes and the mass fluxes are more informative. Table 1 shows the difference in the Darcy flux and in the mass flux for the two situations of no-coupling (NC), and non-iterative coupling (NIC). Iterative coupling (IC) is not considered because the solutions are at steady state, hence, it is equivalent to NIC. The difference in the Darcy flux between Column 2 and Column 3 is in the ratio of 1.03 which is the value of β . The mass flux, which is obtained by multiplying the Darcy flux by β , is 1.0609 larger for NIC than for NC. Based on this, we consider that coupling between the water flow and the salt transport is a necessary condition for correct fluxes at steady state regime.

5.2. Application 2

This case illustrates the effects of density dependence on variably saturated flow in transient regime.

We assume that initial and BC for pressure heads are given by

$$\Psi(t=0, z) = -100 \text{ cm}; \Psi(t, z=0) = -100 \text{ cm}; \Psi(t, z=L=100 \text{ cm}) = +100 \text{ cm}$$

Two situations are considered for the initial and boundary conditions for concentration.

5.2.1. Application 2-a: Initial fresh water distribution and incoming saltwater.

$$c(t=0, z) = 0.0; c(t, z=0) = 0.0; c(t, z=100 \text{ cm}) = 1.0$$

For all the dependent variables that were considered (pressure head, concentration, and Darcy's flux), the difference between NIC (Non-Iterative Coupling) and IC (Iterative Coupling, nine iterations) was one to two orders of magnitude less than the difference between NIC and NC (No-Coupling). This means that partial coupling (or NIC) is sufficient to simulate seawater concentrations and that iterative coupling (IC) increases the computational cost without increasing significantly the accuracy of the solution. Thus, for the remainder of this paper, density dependence will be simulated only by the NIC scheme.

The pressure head distribution with depth for NC and NIC at $t = 400$ s are shown in Fig. 5. The concentration distribution obtained from NC is also shown. The concentration

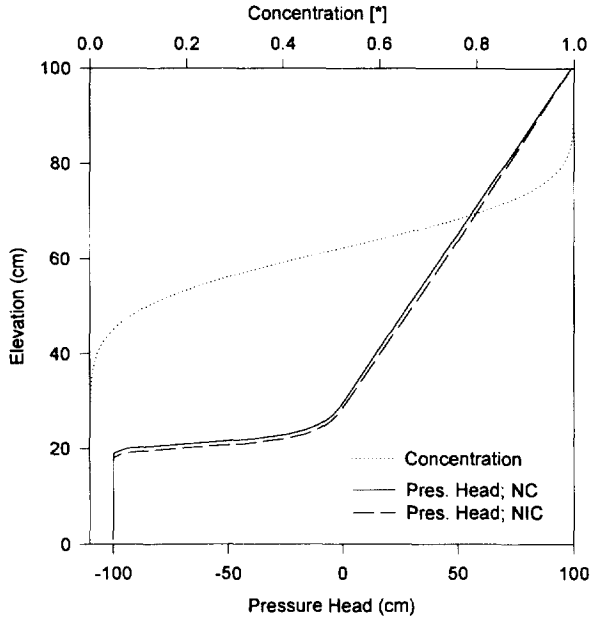


Fig. 5. Concentration and pressure head distributions at $t = 400$ s for Case 2a.

from NIC was not plotted because the scale of the figure does not allow distinction between the two concentration distribution. Fig. 5 shows that the concentration front propagated following the pressure head front. It also shows that the pressure head front for NIC propagated faster than the pressure head front for NC. The difference in arrival times of pressure head fronts and the concentration fronts at $t = 400$ s was much larger than at $t = 50$ s (not shown). The increase is due to an increased amount of salt entering the system behind the pressure head front. Because physical dispersion increases with distance from the source (Bear and Verrujit, 1987), it was expected to have increased the speed of the propagation of the pressure front for NIC relative to NC. For this reason we ran the code for NIC with the dispersivity set to $a_L = 10.0$ cm which is ten times larger than a_L used before, thus increasing drastically physical dispersion. Fig. 6 shows a comparison between pressure head fronts for NIC with $a_L = 1.0$ cm, NIC with $a_L = 10$ cm, and NC. Notice that a_L need not to be changed for NC because the salt transport model is uncoupled from the flow model. As seen in Fig. 6, the pressure head front for NIC $a_L = 10.0$ cm, is actually propagating slower than NIC, $a_L = 1.0$ cm. This is because as seen in Fig. 6, the concentration front for NIC, $a_L = 10.0$ cm propagated faster than the pressure front, causing a zero concentration gradient across the pressure head front. The absence of the concentration gradient across the pressure head front resulted in a reduction in the total head gradient. It is important to note that the amount of salt in the system for NIC $a_L = 10.0$ cm is much larger than for NIC with $a_L = 1.0$ cm; however, it is the position of the salt with respect to the pressure head front that affects the water flow. The reader must be aware that the value $a_L = 10$ cm is not a physically realistic value because the dispersivity

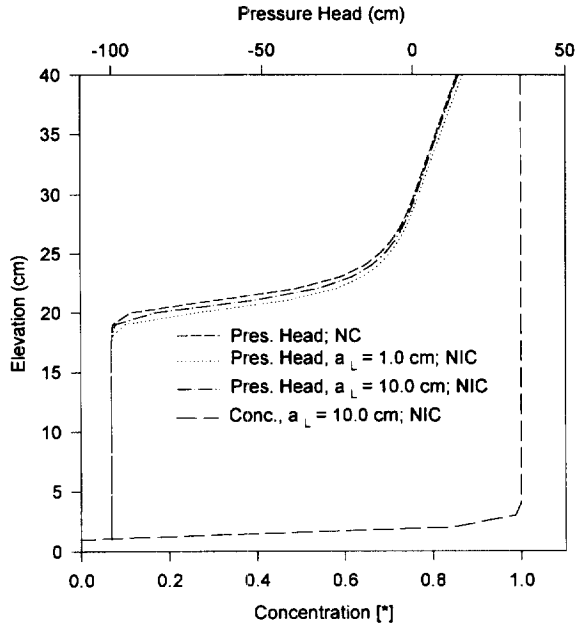


Fig. 6. Relative position of pressure head and concentration fronts for a large dispersivity.

is a scale-dependent parameter. Nevertheless, the use of a large dispersivity provided us with the important information that the relative position of the pressure and the concentration fronts has more effects on the flow than the total salt mass in the system. This has very practical implications, for example, on the transport of the dissolved nutrients in the highly dynamic beach environment where, due to tidal and wave actions, the pressure fronts and the concentration fronts are in constant motion with respect to one another (Wrenn et al., 1997).

The variation of Darcy's flux with time followed closely the variation of the pressure head front and is shown in Fig. 7a and Fig. 7b for $z = 80$ cm and $z = 20$ cm, respectively. In Fig. 7a, the Darcy's flux increased sharply with time and then decreased smoothly towards a steady state value. This is attributed mainly to a large pressure gradient at a near-saturation, thus large, value of the hydraulic conductivity. As seen in Eq. (5), the Darcy's flux is the product of the hydraulic conductivity and the sum of the pressure and gravity gradients. When the pressure head front approached $z = 80$ cm, the pressure gradient was extremely large while K , as given by Eqs. (7a), (7b) and (7c), was very small due to the negative pressure head. The pressure head then increased from -100 cm to near 0.0 cm (not shown) causing the soil moisture ratio and K to increase to near 1.0 and K_0 , respectively. While pressure gradient is still large, K is almost at its maximum. It is at this specific moment that the Darcy's flux, as given by Eq. (5), increased to its peak value. It decreased later because, while K is at its maximum, the pressure head gradient was decreasing towards the steady state value imposed by the boundary conditions. The difference in the arrival times of the Darcy's flux front for NC and NIC is very small at

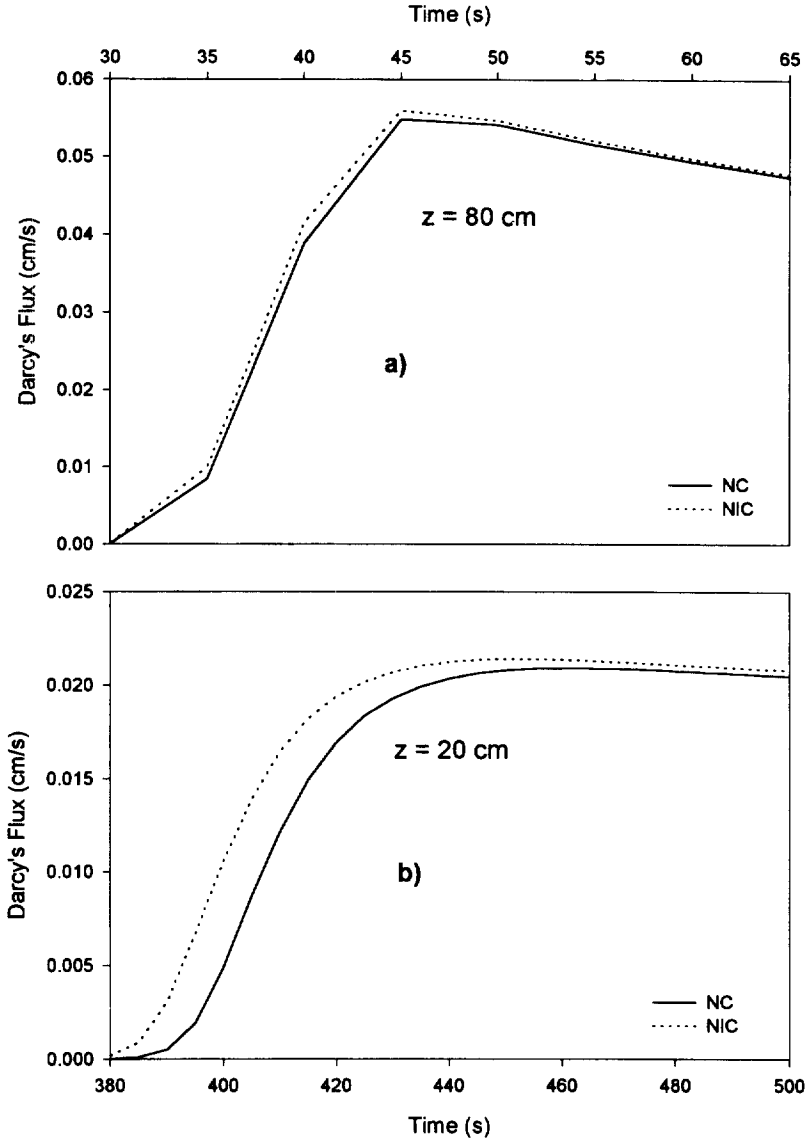


Fig. 7. Variation of the Darcy flux for NC and NIC: a) at $z = 80$ cm, and b) $z = 20$ cm.

$z = 80$ cm as shown in Fig. 7a. However, it is about 10 s at $z = 20$ cm, Fig. 7b. The maximum value of the Darcy's flux at $z = 20$ cm is about 0.020 cm s^{-1} , which is considerably smaller than the maximum value of Darcy's flux at $z = 80$ cm. This is due to the fact that the pressure head gradient for the latter is approaching the steady state. At $t = 50$ s, the pressure head varied from 0 cm to -100 cm over only 3 cm (not shown) while at $t = 400$ s the same variation occurred over 10 cm, thus causing a lower pressure gradient

and consequently a smaller Darcy's flux. In Fig. 7a, the maximum NIC Darcy's flux is about 2% larger than the maximum NC Darcy's flux, whereas in Fig. 7b, the maximum Darcy's flux for NIC is 2.4% larger than its counterpart for NC. This is less than the steady state difference of 3.0% seen in Application 1-a. Thus, there is an increase in the effects of density dependence when approaching a steady state.

5.2.2. Application 2-b: Initial saltwater distribution and incoming fresh water.

$$c(t=0, z)=1.0; c(t, z=0)=1.0, c(t, z=10 \text{ cm})=0.0$$

In this application, the density gradient opposes the pressure gradient. The pressure head front for NIC is retarded with respect to the pressure head front for NC, as shown in Fig. 8 at $t = 400$ s. The difference in the time of arrival between NC and NIC for this case is smaller in magnitude than Application 2-a because, unlike Application 2-a, the density gradient here is opposing the pressure gradient resulting in a decreased total head gradient. The Darcy flux for NIC (at $z = 20$ cm) is retarded relative to the Darcy flux for NC (Fig. 9). It is also reduced in magnitude where the ratio of the maximum value of Darcy's flux of NIC over the maximum value of Darcy's flux for NC is about 1.0%.

6. Conclusions

The effects of salt density on water flow in the unsaturated zone of porous media were

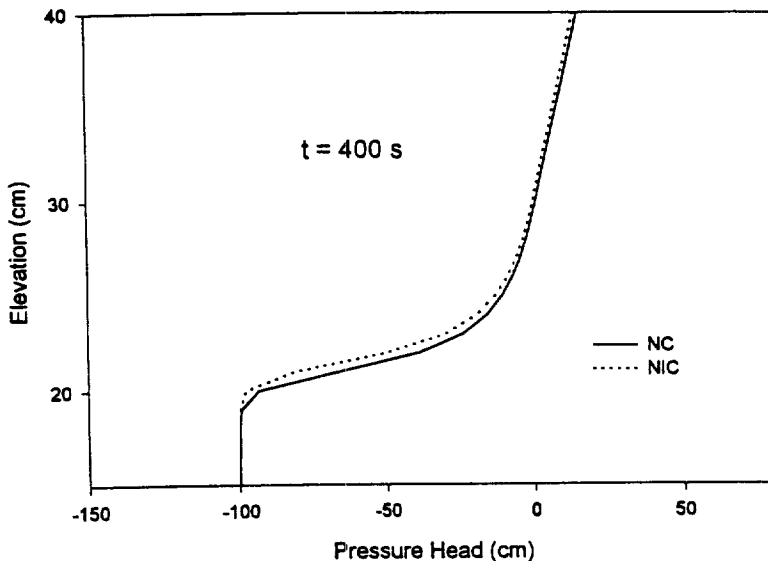


Fig. 8. Pressure head distributions for NC and NIC for Case 2b.

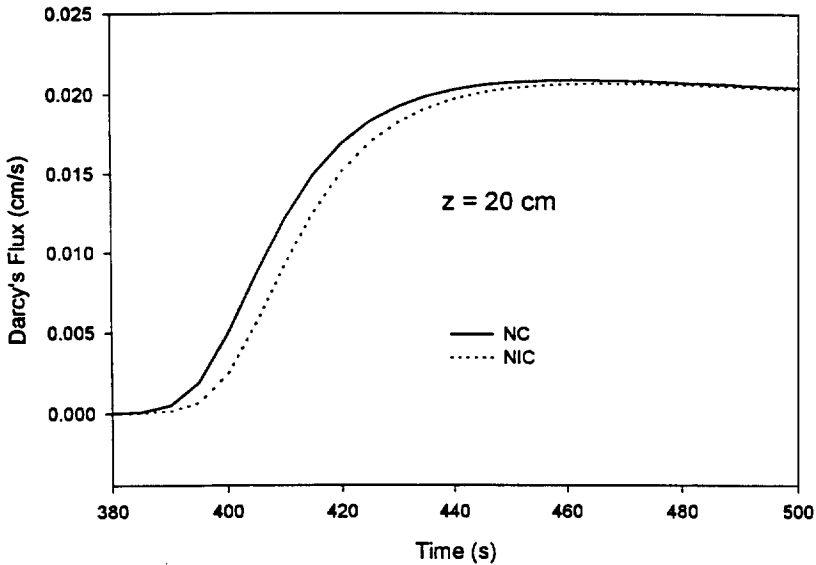


Fig. 9. Darcy fluxes distributions for NC and NIC at $z = 20$ cm.

considered under one-dimensional scenarios. Solutions obtained from uncoupling the flow and the transport equation (no-coupling) were compared to a non-iterative coupling (updating) and to full iterative coupling (nine iterations) and the following conclusions can be drawn:

1. From a numerical standpoint, partial coupling of the flow and transport equations through a noniterative updating procedure yields results that are practically indistinguishable from those obtained using a full iterative coupling of the equations.
2. The coupling of the flow and the transport equations results in a faster propagation (when compared to decoupling whereby the salt acts as a tracer) of the wetting front, the concentration front, and the Darcy flux front and magnitude, when concentrations decrease downward. It results in retardation (relative to decoupling) of these fronts and decrease in the Darcy's flux magnitude when concentrations increase downward. The difference in magnitude between the Darcy's flux for the coupled case and the uncoupled case reaches its maximum at steady state.
3. For the density-dependent flow (coupling), the propagation of the concentration and the pressure fronts are more affected by their position with respect to each other than by the total amount of salt in the system. This implies that the effects of salt concentration on water flow in variably-saturated media can be significant in one-dimensional flows. This is because under unsaturated conditions, water flow is predominately vertical, whereas under saturated flow conditions, the horizontal component of the flow can be considerable. This allows the vertical flow of the denser fluid without a corresponding displacement of the resident fluid.

Acknowledgements

This work was supported, by the US Environmental Protection Agency's National Risk Management Research Laboratory, Cincinnati, OH, under Cooperative Agreement No CR-821029. However, it does not necessarily reflect the views of the Agency, and no official endorsement should be inferred.

References

- Abramowitz, M., Stegun, I.A., Handbook of Mathematical Functions. Dover, New York, NY, 1970.
- Anderson D.A., Tannehill, J.C. and Pletcher, R.H., 1984. Computational fluid mechanics and heat transfer, Series in computational methods in mechanics and thermal sciences, NY, p. 600.
- Barry, D.A., Parlange, J.Y., Sander, G.C., Sivaplan, M., 1993. A class of exact solutions for Richard's equation, *J. of Hydrol.*, 142, 29–46.
- Basha, H.A., 1984. Multidimensional steady infiltration with prescribed boundary conditions at the soil surface. *Water Resour. Res.*, 30: 2105–2118.
- Bear, J., Verrujit, A., Modeling groundwater flow and pollution: with computer programs for sample cases. D. Reidel Pub. Co., Dordrecht, volume 27, p. 414.
- Boufadel M.C., Multiple Unit Hydrographs from the Nash Model, Master Thesis, Dep. of Civil and Env. Eng., University of Cincinnati, 1992.
- Bouloutas, E.T., 1989. Improved numerical approximations for flow and transport in the unsaturated zone, Ph.D thesis, Dep. of Civ. Eng., Mass. Inst. of Technol., Cambridge, 1989.
- Bragg J. R., R. C. Prince, E. J. Harner, R. M. Atlas, Bioremediation effectiveness following the *Exxon Valdez* spill, *Proc. 1993 Int. Oil Spill Conference*, pp. 435–447, American Petroleum Institute, Washington DC, (1993).
- Broabridge, P., White, I., 1988. Constant rate rainfall infiltration, a versatile nonlinear model. part 1: analytical solution, *Water Resour. Res.*, 24, 145–154.
- Brooks, R.H., Corey, A.T., 1966. Properties of porous media affecting fluid flow. *J. of Irrig. Drain. Div., Am. Soc. Civil Eng.*: 92(IR2): 61–88.
- Brutsaert, W., 1982. Some exact solutions for nonlinear desorptive diffusion, *J. of Appl. Math. Phy.*, 33, 540–546.
- Celia, M.A., Bouloutas, E.T., Zarba, R.L., 1990. A general mass-conservative numerical solution for the unsaturated flow equation, *Water Resour. Res.*, 26, 1483–1496.
- Cooley, R.L., 1983. Some new procedures for numerical solution of variably saturated flow problems, *Water Resour. Res.*, 19, 1271–1285.
- Cox, C.L., Jones, W.F., Quisenberry, V.L., Yo, F., 1994. One dimensional infiltration with moving finite elements and improved soil diffusivity, *Water Resour. Res.*, 30, 1431–1438.
- CRC Handbook of Chemistry and Physics, 63rd edn., Boca Raton, 1982–83.
- Frind E.O., 1982a. Simulation of long-term transient density-dependent transport in groundwater. *Adv. Water Resour.*, 5: 73–88.
- Frind E.O., 1982b. Seawater intrusion in continuous coastal aquifer-aquitard systems. *Adv. Water Resour.*, 5: 89–97.
- Galeati, G., Gambolati, G., 1989. On boundary conditions and point sources in the finite element integration of the transport equation, *Water Resour. Res.*, 25, 847–856.
- Galeati, G., Gambolati, G., Neuman, S.P., 1992. Coupled and partially coupled Eulerian-Lagrangian model for freshwater, *Water Resour. Res.*, 28 (1), 149–165.
- Gureghian A.B., TRIPM: A two-dimensional finite-element model for the simultaneous transport of water and reacting solutes through saturated and unsaturated porous media, Technical Report, Battelet memorial institute, Columbus, 1983.
- Henry H.R., Effects of dispersion on salt encroachment in coastal aquifers, *Sea Water in Coastal Aquifers*, U.S. Geol. Surv. Water Supply Pap., 1613-C, 70–84, 1964.

- Huyakorn P.S., and Pinder, G.F., 1983. *Computational Methods in Subsurface Flow*, Academic Press, New York, p. 473.
- Huyakorn, P.S., Springer, E.P., Guvanasen, V., Wadsworth, T.D., 1986. A three-dimensional finite element model for simulating water flow in variably saturated porous media, *Water Resour. Res.*, 22, 1790–1808.
- Huyakorn, P.S., Andersen, P.F., Mercer, J.W., White, H.O. Jr., 1987. Saltwater intrusion in aquifers: Development and testing of a three-dimensional finite element model, *Water Resour. Res.*, 23, 293–312.
- Istok, J., *Groundwater Modelling by the Finite Element Method*. American Geophysical Union, Washington, 1989.
- Kirkland, M.R., Hills, R.G., Wirenga, P.J., 1992. Algorithms for solving Richards' equation for variably saturated soil, *Water Resour. Res.*, 28, 2049–2058.
- Lomen, D.O., Tonellato, P.J., Warrick, A.W., 1984. Salt and water transport in unsaturated soil for non-conservative systems, *Agr. Water Mgmt.*, 8, 397–409.
- Neuman, S.P., 1973. Saturated-unsaturated seepage by finite elements, *J. Hydraul. Div. Am. Soc. Civ. Eng.*, 99 (HY12), 2233–2250.
- Ogata, A., Banks, R.B., A solution of the differential equation of longitudinal dispersion in porous media, Geological Survey Professional Paper 411-a, Washington, 1961.
- Pan, L., Wierenga, P.J., 1995. A transformed pressure head-based approach to solve Richard's equation for variably-saturated soils, *Wat. Resour. Res.*, 31 (4), 925–935.
- Paniconi, C., Putti, M., 1994. A comparison of Picard and Newton iteration in the numerical solution of multi-dimensional variably saturated flow problems, *Water Resour. Res.*, 30, 3357–3374.
- Paniconi C., Aldama, A.A., Wood, E.F., 1988. Time-discretization strategies for the numerical solution of the nonlinear Richard's equation. *Comput. Methods in Subsurface Hydrology*, 161–167.
- Piver, W.T., Lindstrom, F.T., 1991. Numerical methods for describing chemical transport in the unsaturated zone of the subsurface, *J. of Contaminant Hydrol.*, 8, p243–262.
- Rathfelder, K., Abriola, L.M., 1994. Mass conservative numerical solutions of the head-based Richards equation, *Wat. Resour. Res.*, 30 (9), 2579–2586.
- Ronen, D., Yechieli, Y., Shatkay, M., 1996. Characterization of water and solute transport in the unsaturated zone of a hypersaline environment, *Water Resour. Res.*, 32(11): 3267–3275.
- Rossi, C., Nimmo, J.R., 1994. Modeling of soil water retention from saturation to oven dryness, *Wat. Resour. Res.*, Vol 30, No., 3, p701–708.
- Segol, G., Pinder, G.F., 1976. Transient simulation of saltwater intrusion in southeastern Florida, *Water Resour. Res.*, 12: 65–70.
- Usseglio-Polatera, J.M., Aboujaoude', A., Molinaro, P., Rangogni, R., 3-D modelling of coupled groundwater flow and transport within saturated and unsaturated zones, *Computational methods in subsurface hydrology*, M.A. Celia (editor) Elsevier p.169–174, 1990.
- van Genuchten, M.T., 1980a. A closed-form equation for predicting the hydraulic conductivity of unsaturated soil, *Soil Sci. Soc. Am. J.*, 44: 892–898.
- van Genuchten, M.T., 1980b. A comparison of numerical solutions of the one-dimensional unsaturated-saturated flow and mass transport equations, *Finite Elements in Wat. Resour.*, S. Y. Wang et al, Rope Printing Co., Inc., FL, p. 3.49–3.66.
- van Genuchten, M.T., 1981. Analytical solutions for chemical transport with simultaneous adsorption, zero-order production and first-order decay, *J. Hydrol.*, 49: 213–233.
- van Genuchten, M.T., 1983. An hermitian finite element solution of the two-dimensional saturated-unsaturated flow equation, *Advances in Water Resources*, 6: 106–111.
- Venosa, A., Suidan, M.T., Wrenn, B.A., Strohmeier, K.L., Haines, J.R., Eberhart, B.L., King, D., and Holder, E., 1996. Bioremediation of an experimental oil spill on the shoreline of delaware bay, *Env. Sci. Tech.*, 30(5): 1764–1775.
- Voss, C.I., 1984. SUTRA: A finite-element simulation model for saturated-unsaturated, fluid-density dependent groundwater flow with energy transport of chemically-reactive simple-species solute transport, *U. S. Geol. Surv. Water Resour. Invest.*, 84–4369, 409 pp.
- Warrick, A.W., Islas, A., Lomen, D.O., 1991. An analytical solution to Richard's equation for time varying infiltration, *Water Resour. Res.*, 27 (5), 763–766.
- Wierenga, P.J., van Genuchten, M.T., 1989. Solute transport through small and large unsaturated soil columns, *Ground Water*, 27, 35–42.

- Wise, W.B., Guven, O., Molz, F.J., 1994. S. C. McCutcheon, High-permeability, oil-fouled beach, *ASCE Journal of Env. Eng.*, 120, 1361–1379.
- Wrenn, B.A., Suidan, M.T., Strohmeier, K.L., Eberhart, B.L., Wilson, G.J., Venosa, A.D., 1997. Nutrient transport during bioremediation of contaminated beaches: Evaluation with Lithium as a conservative tracer, *Water Res.*, 31(3):515–524.
- Xue, Y., Xie, C., Wu, J., Liu, P., Wang, J., Jiang, Q., 1995. A three-dimensional miscible transport model for seawater intrusion in China, *Water Resour. Res.*, 31 (4), 903–912